Submitted Manuscript: Confidential
Template revised July 2024

Scalable detection of cellular protein-small molecule interactions via fluorescence anisotropy

Qing Tang[1,2†], Yuan-Ping Wei[1,3†], Ricky Ruiqi Ma[1,4†], Na Wei[1,5], Tammy Zihan Zhou[1], Hilary Kung-Yu Ho[1,6], Zafar Iqbal Bhat[1,7], Iqra Ishrat[1,6], Xiaoyu Li[3], Judy Wai Ping Yam[4], Yung Hou Wong[2,9], Qiankun Wang[8], Justin L. Tan[1,5]*

Affiliations:

[1]Institute of Cancer Research, High Throughput Screening Center, Shenzhen Bay Laboratory; Shenzhen, 518132, China.

[2]Division of Life Sciences and the Biotechnology Research Institute, Hong Kong University of Science and Technology; Hong Kong, 999077, China.

[3]Department of Chemistry and State Key Laboratory of Synthetic Chemistry, The University of Hong Kong, Pokfulam Road, Hong Kong SAR, China
Laboratory for Synthetic Chemistry and Chemical Biology Limited, Health@InnoHK, Innovation and Technology Commission, Units 1503-1511, 15/F., Building 17W, Hong Kong SAR, China

[4]Department of Pathology, School of Clinical Medicine, The University of Hong Kong, Hong Kong, 999077, Hong Kong.

[5]School of Basic Medical Sciences, Capital Medical University; Beijing, 100069, China.

[6]School of Chemical Biology and Biotechnology, Shenzhen Graduate School, Peking University; Shenzhen, 518055, China

[7]School of Life Sciences, University of Science and Technology of China; Hefei, 230027, China.

[8]Institute of Infectious Diseases, Shenzhen Bay Laboratory; Shenzhen, 518132, China.

[9]State Key Laboratory of Molecular Neuroscience and the Molecular Neuroscience Center, Hong Kong University of Science and Technology; Hong Kong, 999077, China

*Corresponding author. Email: justintanlab@gmail.com

†These authors contributed equally to this work.

Abstract: Proteolysis Targeting Chimera (PROTACs) are a revolutionary drug modality that can expand the repertoire of druggable targets to proteins lacking conventional active sites or binding pockets[1]. However, the majority of PROTACs developed are against already drugged targets[2] suggesting it is challenging to discover novel binders of undruggable targets. To overcome this, we developed a scalable, efficient, and accessible method to detect cellular protein-small molecule interactions. Cellular Fluorescence Anisotropy (CFAST) measures cellular protein levels through changes in fluorescence anisotropy of a triangulenium dye-labeled nanobody probe. Centrifugation and nuclease incubation remove unwanted cellular components. We demonstrate that CFAST robustly detects cellular PARP1, MK2, and EGFP protein levels. Small molecule incubation, followed by heating and centrifugation, enables detection of cellular protein-small molecule interactions through thermal stabilization of the target protein. CFAST successfully detects cellular PARP1 and MK2 inhibitor binding in a dose-response manner. High-throughput CFAST screening identified a small molecule binder of undruggable transcription factor SOX2. This screening method also enabled development of a bifunctional PROTAC that simultaneously degrades membrane-bound oncogene EGFR and inhibits immune modulating target HRH1. CFAST takes a minimum of 2-3 hours to execute. It utilizes common lab equipment and reasonably priced reagents. Our work suggests that CFAST is a viable method to enhance drug and probe

discovery through scalable, fast, and economical detection of cellular protein-small molecule interactions.

Introduction:

Proteolysis Targeting Chimera (PROTACs) are a revolutionary new drug modality[3]. PROTACs are bifunctional small molecules comprising two moieties, an E3 ligase binder covalently linked to a binder of a protein target of interest, also known as the warhead. These molecules bring the target protein in close proximity to the E3 ligase, promoting targeted ubiquitination of the protein. This marks the protein for proteasomal degradation[4]. Since this degradation is independent of protein activity, warheads can be designed to bind protein regions outside of conventional active sites or binding pockets. This increases the repertoire of proteins that can be drugged by degradation rather than traditional inhibition[5]. However, current efforts on PROTAC development have focused on already drugged proteins[2]. This suggests that discovering and developing warheads against undruggable proteins remains a challenge.

A reason for challenging warhead discovery against undruggable proteins is the lack of suitable assays. Various biochemical assays have been developed to identify protein-small molecule binding[6], but most are performed *in vitro*. These assays require costly instrumentation as well as purified proteins, and do not assess cell permeability or biological activity. In contrast, cell-based assays validate these aspects but often fail to confirm cellular target engagement[7]. An assay combining the advantages of biochemical and cell-based methods could reduce the costs and challenges associated with drug discovery. The Cellular Thermal Shift Assay (CETSA) measures cellular protein-small molecule interactions via thermal stability and Western blotting[8], but its inapplicability to high-throughput screening necessitates the development of scalable methods, such as the CETSA screen technology using AlphaLISA proximity labeling[9]. However, the utility of CETSA screening is constrained by target proteins that form dimers, and the requirement of two separate antibodies that bind the dimer in sufficiently close proximity for signal emission. An alternative to CETSA screening is SplitLuc CETSA, which links the target protein to a split luciferase system that induces luminescence when the target protein is thermally stabilized by small molecule binding[10]. However, SplitLuc CETSA requires genetic modification of cells and only one target can be assessed at a time. There is room to innovate on current methods for novel PROTAC discovery.

To provide an alternative scalable, efficient, and accessible method for small molecule drug discovery, we developed Cellular Fluorescence Anisotropy (CFAST). CFAST innovates on fluorescence anisotropy (FA) and altered protein thermal stability by small molecule binding. FA measures plane-polarized fluorescence emission differences in perpendicular planes when a fluorescent molecule tumbles at different rates[11]. This method typically assesses binding between a protein-of-interest and a dye-labeled small molecule probe. Higher FA, measured in milli-polarization units (mP), is proportional to an increase in molecular mass of the probe complex[12]. However, FA is typically performed *in vitro* due to a high background caused by viscosity of more complex solutions[13]. In addition, FA is limited to targets with known small molecule binders to act as probes. Probes are typically of smaller masses to increase the sensitivity of detection[14]. To overcome the aforementioned limitations, we employed long lifetime triangulenium dye-labeled nanobody probes[15–17], as well as nuclease incubation and centrifugation steps, to enable FA to quantify native, soluble cellular protein in lysates. CFAST robustly detects endogenous PARP1, MK2, and EGFP protein levels after a short 3-hour protocol. Small molecule incubation followed by heating and centrifugation allows for detection of protein-small molecule interactions. We demonstrate that CFAST can identify PARP1 inhibitor olaparib and MK2 inhibitor PF-3644022 interactions with their endogenous target proteins in a dose-response manner. Additionally, CFAST enables absolute quantification of cellular PARP1 using known standards. We optimized

CFAST for high-throughput screening in 384-well plates in less than 10 hours, screening a library of ~900 approved drugs, active pharmaceutical ingredients, and synthetic compounds on HEK293T cells expressing tagged SOX2 or EGFR. SOX2 is an undruggable transcription factor while EGFR is a membrane-bound oncogene. We identified wedelolactone as a novel SOX2 binder. In addition, we also identified HRH1 inhibitor desloratadine as an EGFR binder. From this binder, we developed a bifunctional PROTAC that simultaneously degrades EGFR and inhibits HRH1, which has recently been shown to modulate an immune checkpoint[18]. Our results indicate that CFAST is a scalable, practical, and broadly applicable technique that could assist PROTAC development against novel targets.

Results:

Long lifetime fluorescent dye labeled nanobody probes can detect cellular protein levels.

To develop a technology that can robustly identify cellular protein-small molecule interactions, we first devised a way for scalable and broadly applicable cellular protein detection. We hypothesized that a long life-time triangulenium dye-labeled nanobody probe would overcome the size limit for FA probes, and have sufficient dynamic range to quantify a specific protein-of-interest by measuring FA changes upon nanobody-protein target binding. Hence, we synthesized diazaoxatriangulenium (DAOTA)-labeled nanobody probes targeting PARP1 and MK2, with EGFP as a control probe for non-specific binding. We tested all probes with their respective recombinant protein targets. Significant, dose-dependent changes in FA were observed when PARP1 probe was incubated with recombinant PARP1 protein, but not with EGFP probe (Fig. S1A). We also observed a similarly significant response for MK2 probe incubated with recombinant MK2 protein, but not when PARP1 and EGFP probes were used (Fig. S1B). These results suggest an acceptable degree of *in vitro* specificity of our probes.

Next, we devised a protocol that enabled our probes to detect cellular protein with the minimum number of steps. Freeze-thaw cycles were used to lyse cells, followed by centrifugation to remove insoluble material. Probe was then incubated with the resultant supernatant, after which FA was measured. We tested this protocol to detect cellular MK2 in wildtype (WT) HEK293T cells and HEK293T cells overexpressing MK2. To minimize effects from non-specific probe binding, we added a control EGFP probe to every sample for normalization. Initial results showed high background in our FA readings compared to *in vitro* results (Fig. S1B and S2A). We suspected that this was due to the presence of soluble nucleic acids which contributed to an unacceptably high viscosity of the solution. By adding an incubation step with a nuclease that digests both DNA and RNA, we significantly reduced the background FA, allowing for robust quantification of MK2 (Fig. S2A). We conducted similar experiments to quantify endogenous PARP1 in WT Hela cells and Hela cells with PARP1 knockout (KO). Interestingly, nuclease incubation had no significant effect on the ability of our probe to quantify PARP1 protein (Fig. S2B). We speculate that this may be related to the size of the PARP1 protein, which has a higher molecular weight of 110 kDa compared to MK2, which has a lower molecular weight of approximately 44 kDa. Our results suggest that with smaller protein targets, nuclease incubation is recommended as viscosity affects the dynamic range of the FA readout. However, for detecting larger protein targets, viscosity has minimal effect and nuclease incubation is optional.

CFAST can quantify absolute cellular protein

We applied our optimized CFAST protocol (Fig. S3) as an alternative to immunoblotting to detect cellular protein levels of EGFP, PARP1, and MK2 protein. In HEK293T and HEK293T expressing EGFP cells, CFAST could robustly detect high levels of EGFP in the EGFP-expressing line, with no changes observed in PARP1 (Fig. S4A). We also observed the expected trend of high FA signal for MK2 in MK2 overexpressing cells and low PARP1 signal in KO cells compared to controls, with minimal detection in the EGFP control probe samples (Fig. S4B and S4C). We validated that protein levels in the various cell lines by Western blot, which tallied with their respective CFAST readouts (Fig. S4D-F). These results suggest that CFAST can detect changes in cellular protein levels.

Since our CFAST measurements vary proportionally with the amount of protein target, we examined if this method could be used for absolute protein quantification. To quantify the amount of PARP1 protein in Hela cells, we first generated a standard curve. We measured the FA of PARP1 probe added to varying amounts of recombinant PARP1 protein, dissolved in equal amounts of Hela KO PARP1 cell lysate (Fig. S5A). The presence of Hela lysate devoid of PARP1 in the standard curve measurements accounts for the background viscosity due to the cellular composition of Hela cells. This allows for a more accurate comparison to CFAST measurements of endogenous PARP1 in WT Hela cells (Fig. S5B). For these endogenous measurements however, adding more Hela cells would alter the background cellular composition of each measurement. Hence, similar to the standard curve, we added decreasing amounts of Hela KO cell lysate to increasing amounts of WT Hela lysates. This ensured a balanced cellular composition, with the only variable being the amount of endogenous PARP1 protein (Fig. S5C). Based on our readings, we calculated the absolute amount of PARP1 protein as 0.879 ± 0.081 ng/μg of Hela cell lysate (Fig. 5D). This result closely aligns with previous findings from a study that utilized mass spectrometry for quantification[19], validating the acceptable accuracy of our results. Out data suggest that CFAST can robustly determine the relative and absolute abundance of a range of cellular proteins-of-interest.

CFAST combined with thermal stability enables cellular protein-small molecule interaction detection

To enable CFAST detection of cellular protein-small molecule interactions, we incorporated a small molecule incubation and heating step to the protocol (Fig. S6). This allows for drug incubation in live cells to engage and stabilize cellular protein targets, so when heat is applied to denature proteins, more drug-bound protein remains in its native soluble state. Optional nuclease incubation and centrifugation are then applied to reduce solution viscosity and remove insoluble material. CFAST probes can then be applied to quantify the amount of stabilized protein as a proxy for the degree of small molecule-cellular protein target engagement (Fig. 1A). We applied this modified protocol to live HEK293T cells incubated with a fixed concentration of known PARP1 inhibitor olaparib and processed at different temperatures. CFAST detected a significant increase in the thermal stability of cellular PARP1 owing to olaparib binding (Fig. 1B). In addition, CFAST could quantify the interaction between cellular PARP1 and olaparib in a dose-dependent manner (Fig. 1C). CETSA performed in a similar temperature gradient and dose-response fashion for PARP1 and olaparib recapitulated our CFAST results (Fig. 1D and 1E). Further, we tested 6 additional PARP1 inhibitors and demonstrated significant CFAST detection of their association with cellular PARP1, in concordance with CETSA (Fig. 1F and 1G). DMSO and non-PARP1

binder metoclopramide expectedly showed negative results. To assess the applicability of small molecule binding detection by CFAST to other proteins, we treated HEK293T cells overexpressing MK2 with known MK2 inhibitor PF-3644022. Similar to PARP1, CFAST was able to detect increased thermal stability of cellular MK2 with PF-3644022 treatment (Fig. 2A) and dose-dependent binding of PF-3644022 to MK2 (Fig. 2B). These MK2 results were comparable with CETSA (Fig. 2C and 2D). Our results suggest that CFAST is a viable alternative for detecting cellular protein-small molecule interactions.

CFAST screening identifies a small molecule binder of undruggable transcription factor SOX2.

We next investigated if CFAST could be scaled for high-throughput screening. First, we tested if CFAST could identify a positive hit from a pool of 5 small molecules. Expectedly, CFAST robustly detected PARP1-olaparib binding in HEK293T cells treated with a pool of olaparib combined with four other drugs, to a similar degree as olaparib treatment alone (Fig. 3A). Next, we adapted our protocol for 384-well format, scaling down reagents and utilizing a lower centrifugation speed (Fig. S7).

We then applied CFAST to screen for small molecule binders of presently undruggable oncogene SOX2[20]. SOX2 is a Yamanaka transcription factor that plays a pivotal role in maintaining pluripotency and self-renewal in stem cells[21]. SOX2 is also implicated in various cancers, where it contributes to tumorigenesis and cancer progression by regulating key signaling pathways[22]. We screened a library of 900 approved drugs and active pharmaceutical ingredients in pools of 5 drugs on HEK293T cells expressing MYC-tagged SOX2, utilizing a MYC-tag nanobody probe for CFAST due to the lack of commercially available SOX2 nanobody. We obtained one hit pool, and further CFAST testing of the individual drugs in the pool identified wedelolactone as a SOX2 binder (Fig. 3B and 3C). We validated that wedelolactone binds SOX2 with a K_d of 5.54 μM via surface plasmon resonance (Fig. 3D and 3E). In addition, CETSA revealed that wedelolactone increased the thermal stability of SOX2 in the H69 cell line, which endogenously expresses SOX2 (Fig. 3F). Wedelolactone, which is derived from the plant wedelia chinensis, has been recognized for its anti-inflammatory and anti-cancer properties[23]. However, there is currently no evidence of wedelolactone binding directly to SOX2. Our data suggests that CFAST can be used to robustly screen for small molecule binders of protein targets, particularly undruggable nuclear targets like SOX2, which can be useful in drug and probe discovery and development.

CFAST screening identifies a small molecule binder of membrane-bound oncogene EGFR.

Since we showed that CFAST can discover binders of an undruggable nuclear protein, we wondered if our method could be useful for membrane protein drug or probe discovery. EGFR is an important membrane-bound protein that triggers oncogenic signaling in cancer. Wildtype and mutant EGFR have been successfully drugged in various cancers, but drug resistance continues to be an issue[24,25]. Novel compounds could be useful in developing next-generation EGFR drugs. We therefore screened our compound library on HEK293T cells expressing MYC-tagged EGFR using EGFR inhibitor gefinitib as control. Unexpectedly, we identified allergy drug desloratadine as a previously uncharacterized EGFR binder (Fig. 4A). We validated that desloratadine binds EGFR with ~677 nM half maximal inhibitory concentration (IC_{50}) via fluorescence polarization (Fig.

S8A). Furthermore, Temperature gradients and dose-response CETSA experiments with desloratadine treatment revealed that this drug stabilizes cellular EGFR (Fig. S8B-D). These data suggest that CFAST successfully identified desloratadine as a novel EGFR binder. CFAST is therefore applicable to membrane protein drug and probe discovery.

Development of a bifunctional EGFR/HRH1 targeting tool compound to simultaneously probe cancer signaling and immune checkpoint inhibition.

While loratadine is primarily used to treat allergies as a potent inhibitor of histamine receptor H1 (HRH1), a recent study concluded that antihistamines targeting HRH1 on tumor-associated macrophages (TAMs) could alleviate immunotherapy resistance in cancer patients[18]. Hence, we wondered if we could repurpose loratadine to develop a bifunctional PROTAC targeting EGFR and HRH1 to simultaneously probe oncogenic signaling and the tumor microenvironment. We synthesized two PROTAC analogs E151 and E152 with a desloratadine warhead and a pomalidomide E3 ligand moiety (Fig. 4B). Both compounds demonstrated dose-dependent depletion of endogenous EGFR in the A431 epidermoid carcinoma cell line, with the Hook effect observed at higher doses (Fig. 4C). EGFR degradation was rapid, with significant reduction observed within 6 hours, and highly potent, with half maximal degradation concentrations (DC_{50}) in the nM range (Fig. 4C). Our results suggest that desloratadine-based PROTACs can potently degrade EGFR.

PROTACs dependence on the ubiquitin-proteasome system for degradation[26]. We therefore performed rescue experiments to validate the mechanism of action of our compounds. Pre-treatment with proteasome inhibitor MG132 abolished EGFR degradation by E151, suggesting that proteasomal activity is required (Fig. 4D). To implicate E3 ligase activity, we inhibited Cullin-RING ligase activity with MLN4924, which blocks neddylation and thus activation of the ligase for ubiquitination. Similar to MG132, MLN4924 treatment blocked E151-mediated degradation, suggesting that neddylation plays a role in the degradation (Fig. 4D). Finally, to provide direct evidence for ubiquitination by the E3 ligase, we performed an EGFR immunoprecipitation assay with E151 treatment. MG132 was added to enhance the signal by inhibiting protein degradation, allowing ubiquitinated protein accumulation. In cells expressing HA-tagged ubiquitin, treatment with E151 increased polyubiquitinated EGFR (Fig. 4E). This data suggests that our compounds degrade EGFR through the ubiquitin-proteasome system.

To assess the biological activity of our compounds, we tested multiple cancer cell lines with varying levels of EGFR expression. Both E151 and E152 altered the viability of cancer cells upon addition to the culture media (Fig. 4F and 4G). This suggests that our compounds are cell permeable. In addition, the compounds showed selectivity for cell lines expressing higher levels of EGFR, with lower half maximal effective concentrations (EC_{50}) values observed (Fig. 4F and 4G). This data suggests that our compounds have biological effects on cancer cells correlating with EGFR expression.

Although we validated that our PROTACs demonstrated potent EGFR degradation activity, it is unclear if the desloratadine warhead still conferred HRH1 degradation or inhibition activity. Since the immunosuppressive effect of HRH1 occurs on TAMs[18], we examined the effect of our compounds on M2-like immunosuppressive induced macrophages derived from the human THP-1 monocytic cell line[27]. We used M1-like induced macrophages, which are immune responsive, as

a control. M1-like macrophages express less HRH1 than M2-like macrophages, similar to prior published work (Fig. S9A and 5A)[18]. In addition, we validated that the M2 induced macrophages expressed the appropriate functional markers (Fig. S9B-F). We then performed membrane protein fractionation after compound treatment to examine membrane-bound HRH1 levels. Interestingly, E151 moderately reduced HRH1 levels at 10 nM, with higher protein levels at higher concentrations likely due to the Hook effect (Fig. 5A). HRH1 inhibitor fexofenadine[28] however, did not alter HRH1 levels (Fig. 5A). This data suggests that our PROTACs might moderately degrade HRH1 in induced macrophages.

We next examined the effects of our compounds on the macrophage immune checkpoint pathway. A key mechanism by which M2 macrophages induce immunotherapy resistance is through the increased expression of membrane-bound checkpoint protein VISTA, which is almost absent in M1 immune responsive macrophages[18]. We therefore examined if our PROTACs had effects on VISTA. Intriguingly, E152 treatment on M2-like induced macrophages could decrease membrane-bound VISTA levels similar to fexofenadine (Fig. 5B). This decrease in HRH1 mimics an M1-like state with low HRH1 expression (Fig. 5B). It is possible that our PROTACs retain the HRH1 inhibitory ability of desloratadine. HRH1 activation by histamine induces calcium mobilization from the endoplasmic reticulum[29]. We therefore utilized a calcium flux assay to assess HRH1 activity in M0 (uninduced THP1 cells), M1, and M2 induced macrophages. The M0 state has low HRH1 expression and serves as a negative control for the experiment (Fig. S9A). As M1-like macrophages express less HRH1 than M2-like macrophages, histamine addition showed increased calcium flux in M2 compared to M1 macrophages (Fig. 5C and 5D). Interestingly, both fexofenadine and E151 significantly inhibited calcium flux, suggesting that they inhibited HRH1 activity (Fig. 5C and 5D). These data suggest that our PROTACs inhibit HRH1 to potentially modulate the macrophage immune checkpoint.

To further validate the effects of our compounds on the macrophages, we assessed the levels of various M1 and M2 markers in M2-like induced macrophages in response to treatment. Both fexofenadine and E151 significantly downregulated M2 markers IL10, MCP1 and ARG (Fig. 5E-G). Interestingly, E151 was more effective than fexofenadine at suppressing these markers at similar doses. We observed a similar trend with E152 treatment, which significantly decreased M2 marker levels (Fig. S9G-J) and concurrently increased M1 marker levels (Fig. S9K and S9L) in a dose-dependent manner. This data suggests that our compounds can convert M2-like induced macrophages to an M1-like state.

Discussion:

CFAST enables FA to measure cellular proteins-of-interest with minimal purification. Since the development of FA as an assay to quantify molecular interactions of biomolecules in the 1950s[30–32], there have been more than 1000 unique examples of FA assays developed, with the vast majority used for high-throughput screening[12]. The traditional FA assay typically involves a purified protein target with a fluorescent dye-labeled probe with known binding affinity to the protein[12]. This limitation precludes the use of FA for quantifying a broad range of proteins and for identifying small molecule binders of undruggable targets. Our CFAST probes are dye-labeled nanobodies, where the nanobody can be chosen based on one's protein-of-interest to be interrogated. In the case where nanobodies against a target of interest is unavailable, one can utilize a tagged version of the protein with a tag-specific nanobody probe as we have done in our SOX2

and EGFR screens. The modularity of CFAST could therefore broaden the utility of FA for drug discovery against a variety of targets.

In addition to potentially broad utility, CFAST is straightforward and cost-effective. This method requires commonly available lab equipment such as centrifuges, heat blocks, thermocyclers, and FA-enabled plate readers. All reagents required are commercially available for a reasonable price. We estimate that in a 384-well screening format, the cost of the assay per sample is about US$0.20. We predict that CFAST will be practical for the majority of research labs, promoting accessible PROTAC discovery and development against new targets of interest. We demonstrate this by performing CFAST screens to identify tool compounds against undruggable transcription factor SOX2 and membrane oncogene EGFR.

Transcription factors and membrane proteins are two classes of challenging proteins to drug. Transcription factors comprise the second largest class of oncogene but are ~85% undruggable[33]. Owing to transcription factors being intrinsically disordered, it is currently difficult to obtain structures or develop in vitro screening assays for effective drug discovery [34]. Similarly, membrane proteins comprise ~60% of possible drug targets. However, owing to the necessity for membrane localization for structural stability and function, structural determination and screening assay development is likewise challenging[35]. As a proof of concept that CFAST can address these drug discovery difficulties, we conducted successful screens against undruggable transcription factor oncogene SOX2 and membrane-bound oncogene EGFR. In terms of SOX2, we posit that our identified tool compound, Wedelolactone, will be useful for developing a targeted SOX2 degrader for probing cancer biology or for drug discovery. With regards to our bifunctional EGFR degrading-HRH1 inhibiting PROTACs, we suggest that these tool compounds can be useful in understanding the synergy of simultaneously targeting oncogenic signaling and modulating a TME immune checkpoint in EGFR-dependent cancers. In addition, these compounds could be used to assess the efficacy of a two-pronged therapy in these cancers. CFAST therefore provides an opportunity to develop PROTACs against challenging targets.

While CFAST is practical, future modifications could improve its resolution. Since certain cellular proteins-of-interest might be expressed at low levels, it will be useful to enhance the ability of CFAST to robustly detect such proteins without overexpressing them. We observed that the accuracy of CFAST is correlated to higher dye-labeling efficiency, which results in higher fluorescence intensity values. It could therefore be useful to develop long life-time fluorophores with higher fluorescence intensities to enable CFAST detection of low abundance proteins. Advances in fluorescence detection instrumentation could also enhance CFAST.

Overall, our data suggests that CFAST is a viable alternative method for PROTAC discovery and development. CFAST combines the advantages of biochemical and cell-based assays into one convenient and cost-effective method. CFAST allows for high-throughput chemical screening campaigns that can identify cell permeable binders of proteins-of-interest. These binders can then be further developed into PROTACs for downstream biological and drug discovery. The simplicity and low cost of this method could potentially make drug discovery more accessible.

Materials and methods:

Lysis buffer: PBS pH 7.2 (Gibco #20012027), 5 mM $MgCl_2$ (Invitrogen #AM9530G), 0.01(v/v) Triton X-100 (Sigma-Aldrich #T8787), protease inhibitor cocktail (Roche #11836170001)

Labeling buffer: PBS pH 7.4 (Gibco #11965092), 5 mM EDTA (Sigma-Aldrich #E8008), 150 mM NaCl (Sigma-Aldrich #S6546).

Reagents

Olaparib (Selleck #S1060), Nutlin3 (TOPSCIENCE #T2158), PF-3644022 (MCE #HY-107427), A771726 (Sigma-Aldrich #100128), Pronethalol (MCE #HY-B1238), DMSO (Aladdin #D103276), Mycophenolic acid (MPA) (Sigma-Aldrich #475913), Fluzoparib (MCE #HY-114778), Rucaparib phosphate (MCE #HY-10617), Veliparib (MCE #HY-10129), Niraparib (MCE #HY-10619), Metoclopramide (MCE #HY-17382), Talazoparib (MCE #HY-16106), Xipamide (MCE #HY-W042301) , Wedelolactone (MCE # HY-N0551) , Doxapram (MCE #HY-B0551) , Palmitoleic acid (MCE #HY-W011873) , Azamethiphos (MCE #HY-114899) , UltraNuclease (Yeason #20156ES60), drug library (Selleckchem #L1300).

Antibodies

ChromoTek PARP1 VHH, recombinant binding protein (Proteintech #xt), ChromoTek GFP VHH, recombinant binding protein (Proteintech #gt), ChromoTek MK2 VHH, recombinant binding protein (Proteintech #mt), ChromoTek Myc VHH, recombinant binding protein (Proteintech #yt), Sox2 Antibody (CST #2748), EGF Receptor (C74B9) Rabbit mAb (CST #2646), PARP1 Polyclonal antibody (Proteintech #13371-1-AP), MAPKAP Kinase 2 Antibody (GENXSPAN #GXP314100), GFP (D5.1) Rabbit mAb (CST #2956S), HRH1 rabbit antibody (Proteintech; 28763-1-AP), EGFR rabbit antibody (Cell Signaling Technology, 4267), VISTA (Selleck, G23H7), ATPase (Beyotime, AF1864), SOD1(Beyotime, AF8028), HA-tag (Sigmaaldrich, SAB5600116), GAPDH (Beyotime, AF0006).

Recombinant proteins

PARP1 Active human (Sigma-Aldrich #SRP0192), Recombinant Human Active MAPKAPK2 (46-end) Protein (R&D Systems #3705-KS), human SOX2 Protein (ReadCrystal #RC-P1511-1), human IL-4 protein (TargetMol, TMPY-01862), human IL-13 protein (TargetMol, TMAB-00049).

Western blotting

Membrane protein was extracted from cell samples by Membrane and Cytosol Protein Extraction Kit (Beyotime). Samples were boiled in 5X SDS-PAGE loading buffer (Beyotime) at 95℃ for 10 mins. The sample can be frozen and stored at -20 ℃ for later use. Proteins were separated by Express Plus PAGE Gels (GenScript) and transferred to a Mini-size PVDF membrane (TransBlot Turbo). Blocking and antibody incubation were performed with Beyotime Quick Block, according to the manufacturer's instruction. Antibody detection was carried out by Clarity Western ECL Substrate (BIO-RAD).

Surface Plasmon Resonance Experiments

Surface plasmon resonance experiments were performed on the Biacore 8K instrument (Cytiva). Recombinant SOX2 (Readcrystal) was immobilized at 25 °C on CM5 Chips (Cytiva) in sodium acetate (pH 4.5 Cytiva). The surface was activated using 400 mM 1-ethyl-3-(3-dimethylaminopropyl)-carbodiimide and 100 mM N-hydroxysuccinimide (Cytiva) (contact time 120 s, flow rate 30 mL/min). The surface was subsequently deactivated by injecting 1 M ethanolamine for 100 s and conditioned by injecting 50 mM NaOH. Dilution of the SOX2 target protein and coupling was performed using a running buffer without DMSO. The SOX2 target proteins were prepared at 50 μg/mL and coupled to the chip to a density between 7149 response

units. The compounds were diluted in running buffer and injected over the immobilized target proteins (concentration range, 0.125-12.5 μM). Sensorgrams from reference surfaces and blank injections were subtracted from the raw data before data analysis using Biacore Insight software. Affinity and binding kinetic parameters were determined by using a 1/1 interaction model, with a term for mass transport included.

Cell Culture

Human embryonic kidney 293T cells (HEK293T cells, ATCC CRL-3216), HEK293T Tg:MK2 and HEK293T Tg:EGFP were cultured in Dulbecco's Modified Eagle Medium (Gibco); Hela (ATCC CRM-CCL-2) and Hela KO PARP (Abclonal) were cultured in Dμlbecco's Modified Eagle Medium; H69 (ATCC HTB-119) were cultured in Roswell Park Memorial Institute (RPMI) 1640 All culture media contain 0.1 g/L L-glutamine and 10% fetal bovine serum (FBS, AusGeneX, Australia), 100 units/mL penicillin and streptomycin (Gibco).

Heterologous protein expression

To generate stable HEK293T *Tg:MK2* and HEK293T *Tg:SOX2/EGFR*-2*Myc-tag cell line, HEK293T cells were cultured in DMEM medium supplemented with 10% FBS and 1X penicillin/streptomycin. 70% confluent HEK293T cells were transfected in Opti-MEM (#31985-088, Gibco) using 3.0 μg of the pCDH-CMV-Homo-MK2-EF1a-puro (IGEbio) or pCDH-CMV-Homo-SOX2-2*Myc-tag-EF1a-puro (IGEbio), 1.5 μg pMD2.G (#12259, Addgene), 1.5 μg psPAX2 (#12260, Addgene), and 13 μL of Lipo2000 (#11668019, Invitrogen) as per protocol. Cells were incubated for 4 hrs and media was replaced. Virus was collected 48 hrs post transfection and filtered through 0.45 μm filter (Merck Millipore), fresh media was added for second viral harvest. Lenti-concentrate virus precipitation (EMB810A-1, Excel Bio) was added and kept overnight at 4 ºC. The next day, the virus pellet was collected by centrifugation at 3000 rpm, 30 min, 4 ºC. After centrifugation, the supernatant was removed, and viral pellet was resuspended in ice cold supplemented media. Concentrated virus was added to the desired cell line with polybrene 8 ug/ml. Puromycin selection was started at 48 hrs post-transduction. After 7 days, cells were collected and allowed to recover for three additional days before further analysis.

CFAST probe synthesis

A. N-Methyl-N-(4-malimide-butyl)-DAOTA-maleimide dye (KU-dyes, KU560-R-6)

Wet the ultrafiltration tube with cold labeling buffer at 5000 rcf for 1.5 hrs at 4 ℃. Add 125 μL nanobody and fill with cold labeling buffer. After mixing, centrifuge with the above conditions. Incubate nanobody and DAOTA-5-maleimide reaction for 2 hrs at room temperature. Remove unreacted DAOTA by processing with dye removal columns (Thermo Scientific #22858). Store labeled nanobody at 4 ℃ for up to one month away from light.

B. N-Methyl-N-(4-malimide-butyl)-DAOTA-NHS dye (KU-dyes, KU560-R-4)

Wet the ultrafiltration tube with cold PBS (pH7.4) at 5000 rcf for 1.5 hrs at 4 ℃. Add 125 μL nanobody and fill with cold PBS. After mixing, centrifuge with the above conditions. Incubate nanobody and DAOTA-NHS reaction for overnight at 4 ℃. Remove excess DAOTA by dye removal columns (Cytiva #28918007). Store labeled nanobody at 4 ℃ for up to one month away from light.

CFAST Protocols:

CFAST workflow for cellular endogenous protein quantification (1.5 ml tube)

1.5 x 10^7 cells were washed with PBS twice. The remaining PBS was then removed after 400 g centrifugation for 5 min. Cell pellets were re-suspended with 300 μL of lysis buffer. Cell suspensions were freeze-thawed three times with liquid nitrogen to lyse the cells. Cell lysate was incubated with UltraNuclease (2 μL per 1 x 10^7cells) for 1.5 hrs at 37 ℃. Next, the lysate was centrifuged at 20,000 g for 20 mins at 4 ℃. The supernatants were transferred to a 384 well plate (Greiner #784076), 10 μL/well. Probe was diluted with lysis buffer (1:500-1:1000) and 5 μL diluted probe was added per well. Mix by gently pipetting and incubate for 10 mins. Fluorescence anisotropy (FA) was detected with a plate reader (Agilent BioTek Synergy Neo2 #N2MABT-SN) 8 times per well and FA was then measured with (EX 530/25, EM 590/35) filters for each sample. The average mP value was plotted for each replicate well.

CFAST workflow for detecting cellular protein-small molecule interactions (1.5 ml tube)

Equal numbers of cells (1.5×10^7) were seeded in 6-well cell culture plates (Biofil #TCP 011006) with the appropriate amount of cell culture medium and incubated with drug for 2 hrs in an incubator. After the cells were harvested, they were washed twice with PBS to remove excess drug and culture medium. Remaining PBS was then removed after 400 rcf centrifugation for 5 min. Cell pellets were re-suspended with 300 μL of lysate buffer. Heat samples at their target-dependent temperatures in a thermocycler (Bio-Rad, CFX96 Deep Well Dx). For PARP1, heat samples at 50 ℃ for 3 mins and then 4℃ for 3 mins. For MK2, heat samples at 54 ℃ for 3 mins and then 4 ℃ for 3 mins. For SOX2, heat samples at 58 ℃ for 5 mins and then 4 ℃ for 3 mins. Next, cell suspensions were freeze-thawed three times with liquid nitrogen to lyse the cells. Cell lysate was incubated with UltraNuclease (2 μL per $1*10^7$ cells) for 1.5 hrs at 37 ℃. Next, the lysate was centrifuged at 20000 g for 20 mins at 4 ℃ to remove insoluble material. The supernatants were transferred to a 384 well plate (Greiner #784076), 10 μL/well. Probe was diluted with lysis buffer (1:500-1:1000) and 5 μL diluted probe was added per well. Mix by gently pipetting and incubate for 10 min. Detect FA with plate reader (Agilent BioTek Synergy Neo2 #N2MABT-SN) 8 times per well and FA was then measured with (EX 530/25, EM 590/35) filters for each sample. The average mP value was plotted for each replicate well.

CFAST workflow for high-throughput screening (384-well plate)

Equal numbers of cells (1×10^6) were seeded in 384-well PCR plates (Biorad #HSP3801) with 25 μL cell culture medium and incubated with drug for 2 hrs in an incubator. After the cells were harvested, they were washed twice with PBS to remove excess drug and culture medium. Remaining PBS was then removed after 400 rcf centrifugation for 5 mins. Cell pellets were re-suspended with 30 μL of lysis buffer. After heating at the target-dependent temperature in a thermocycler for 6 min, the cell suspensions were freeze-thawed three times with liquid nitrogen to lyse the cells. Cell lysate was incubated with UltraNuclease (2 μL per 1 x 10^7cells) for 1.5 hrs at 37 ℃. Next, the lysate was centrifuged at 4000 rpm for 60 mins at 4 ℃ to remove insoluble material. The supernatants were transferred to a 384 well plate (Greiner #784076), 10 μL for experimental probe and another 10 μL for EGFP probe. Probe was diluted with lysis buffer (1:500-1:1000) and 5 μL diluted probe was added per well. Mix by gently pipetting and incubate for 10 mins. FA was detected with a plate reader (Agilent BioTek Synergy Neo2 #N2MABT-SN) 8 times per well and FA was then measured with (EX 530/25, EM 590/35) filters for each sample. The average mP value was plotted for each replicate well.

Chemical synthesis

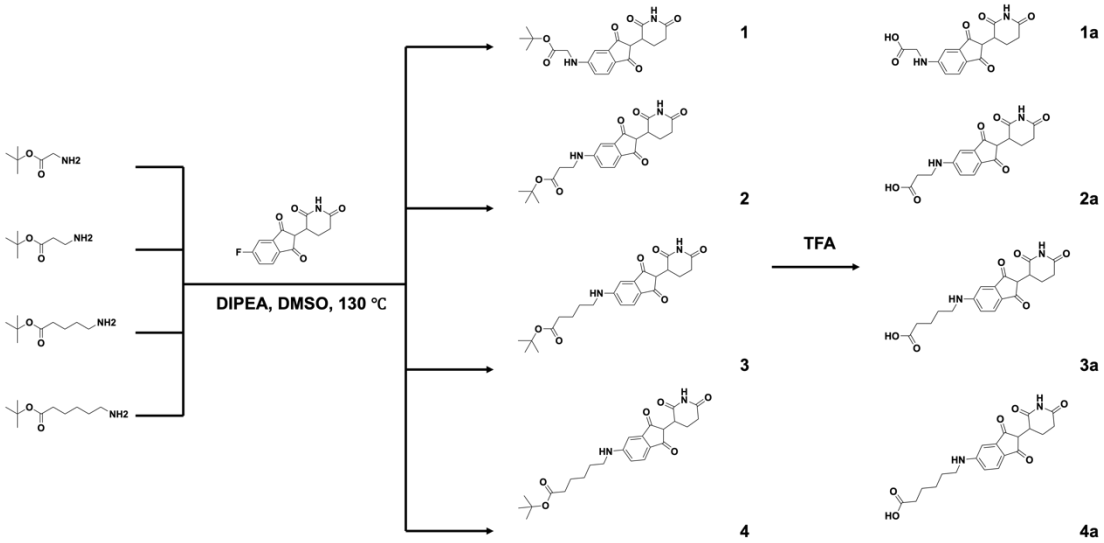

tert-butyl (2-(2,6-dioxopiperidin-3-yl)-1,3-dioxo-2,3-dihydro-1*H*-inden-5-yl)glycinate (1)
tert-butyl 3-((2-(2,6-dioxopiperidin-3-yl)-1,3-dioxo-2,3-dihydro-1*H*-inden-5-yl)amino)propanoate (2)
tert-butyl 5-((2-(2,6-dioxopiperidin-3-yl)-1,3-dioxo-2,3-dihydro-1*H*-inden-5-yl)amino)pentanoate (3)
tert-butyl 6-((2-(2,6-dioxopiperidin-3-yl)-1,3-dioxo-2,3-dihydro-1*H*-inden-5-yl)amino)hexanoate (4)
(2-(2,6-dioxopiperidin-3-yl)-1,3-dioxo-2,3-dihydro-1*H*-inden-5-yl)glycine (1a)
3-((2-(2,6-dioxopiperidin-3-yl)-1,3-dioxo-2,3-dihydro-1*H*-inden-5-yl)amino)propanoic acid (2a)
5-((2-(2,6-dioxopiperidin-3-yl)-1,3-dioxo-2,3-dihydro-1*H*-inden-5-yl)amino)pentanoic acid (3a)
6-((2-(2,6-dioxopiperidin-3-yl)-1,3-dioxo-2,3-dihydro-1*H*-inden-5-yl)amino)hexanoic acid (4a)

4-Fluorothalidomide (124 mg, 0.45 mmol, 1.0 equiv.), amine (0.50 mmol, 1.1 equiv.) and DIPEA (230 µL, 1.35 mmol, 3.0 equiv.) were dissolved in DMSO (1.0 mL, 0.2 M) and warmed to 130 °C for 12 hrs. The residue was purified by flash column chromatography over silica gel, eluted with EtOAc:hexanes (20 –100%) to afford a yellow viscous oil (1-4, 80-90%), then dissolved in 4 ml TFA for 4 hrs to achieve 1a-4a (90%).

3-(5-((2-(4-(8-chloro-5,6-dihydro-11*H*-benzo[5,6]cyclohepta[1,2-*b*]pyridin-11-ylidene)piperidin-1-yl)-2-oxoethyl)amino)-1,3-dioxo-2,3-dihydro-1*H*-inden-2-yl)piperidine-2,6-dione (E151)

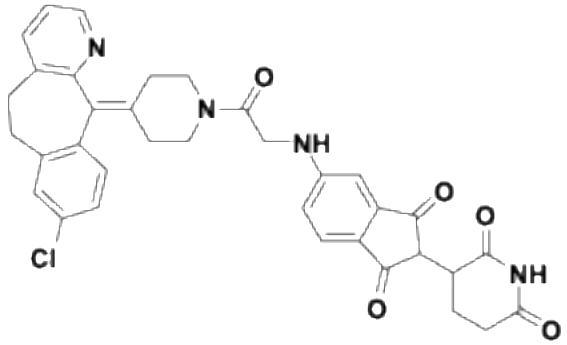

3-(5-((3-(4-(8-chloro-5,6-dihydro-11*H*-benzo[5,6]cyclohepta[1,2-*b*]pyridin-11-ylidene)piperidin-1-yl)-3-oxopropyl)amino)-1,3-dioxo-2,3-dihydro-1*H*-inden-2-yl)piperidine-2,6-dione (E152)

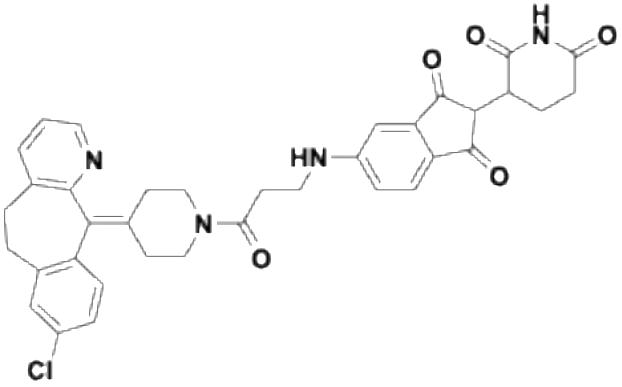

3-(5-((5-(4-(8-chloro-5,6-dihydro-11*H*-benzo[5,6]cyclohepta[1,2-*b*]pyridin-11-ylidene)piperidin-1-yl)-5-oxopentyl)amino)-1,3-dioxo-2,3-dihydro-1*H*-inden-2-yl)piperidine-2,6-dione (E154)

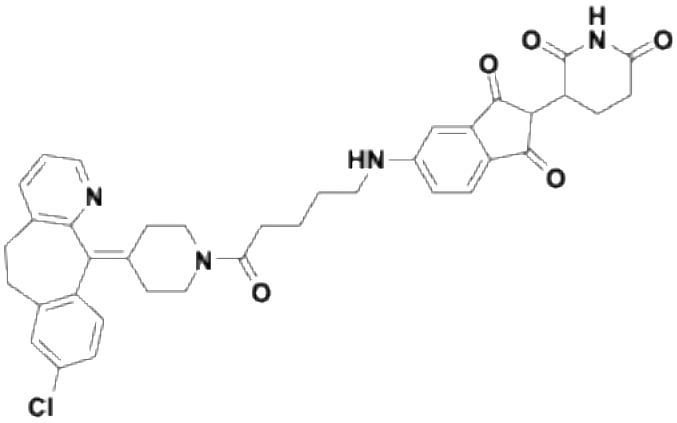

3-(5-((6-(4-(8-chloro-5,6-dihydro-11*H*-benzo[5,6]cyclohepta[1,2-*b*]pyridin-11-ylidene)piperidin-1-yl)-6-oxohexyl)amino)-1,3-dioxo-2,3-dihydro-1*H*-inden-2-yl)piperidine-2,6-dione (E160)

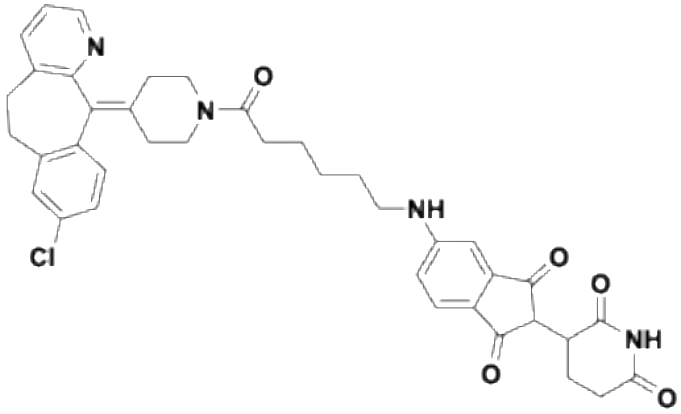

Fluorescence polarization

5-FAM (Bidepharm, BD243928) labeled desloratadine (DL-1, 10 nM) was mixed with increasing concentrations of either recombinant EGFR protein (Sigma, SRP0239) or CA II (MCE, HY-P72860) (0.002–1.5 μM) in a 384-well microplate (Greiner, 784076) and incubated for 30 min at room temperature. EGFR-DL-1 interactions were measured in 50 mM Tris pH 7.5, 100 mM NaCl,

0.1% TCEP and 1% DMSO via fluorescence polarization using the BIOTEK NEO2 microplate reader. Data were plotted and analyzed using GraphPad Prism 10.

Cell viability

Cells were seeded in 96-well plates and treated with E151 or E152 in a variety of doses (0.5-100 μM) after overnight incubation. Cell viability was measured by CellTiter-Glo 2.0 assay (Promega). Luminescence readout (Agilent BioTek Synergy Neo2 #N2MABT-SN) from drug treated wells were normalized against control wells and expressed as percentage cell viability.

Macrophage differentiation

THP-1 monocytic cells were differentiated into macrophages by 24 hr incubation with 150 nM phorbol 12-myristate 13-acetate (PMA, TargetMol, TQ0198) followed by 24 hr incubation in RPMI medium. M1-like macrophages were obtained by incubation with 20 ng/ml of IFN-γ (TargetMol, TMPY-01714) and 10 pg/ml of LPS (TargetMol, T11855). M2-like macrophages were obtained by incubation with 20 ng/ml of interleukin 4 (IL-4) and 20 ng/ml of interleukin 13 (IL-13).

qRT-PCR

Total RNA was extracted using the HiPure Total RNA Kit (Magen, R4111-03). 2 μg total RNA was reverse transcribed using the RevertAid First Strand cDNA Synthesis Kit (Thermo Fisher, K1622). Amplification reaction assays contained 2x SYBR Green qPCR Master Mix (Selleck, B21202) and primers (IGE, 300 nM). ACTB was used as the reference gene for normalization and mRNA abundance was quantified using the threshold cycle method.

Primers	**Forward sequence 5'-3'**	**Reverse sequence 5'-3'**
HRH1	GCTGGGCTACATCAACTCCAC	CCCTTAGGAGCGAATATGCAGAA
TNFalpha	CTCTTCTGCCTGCTGCA CTTTG	ATGGGCTACAGG CTTGTCACTC
CXCL10	GAAAGCAGTTAGCAAG GAAAGGTC	ATGTAGGGAAGT GATGGGAGAGG
CD206	CCATGGACAATGCGCG AGCG	CACCTGTGGCCC AAGACACGT
CD163	TTTGTCAACTTGAGTCC CTTCAC	TCCCGCTACACT TGTTTTCAC
GAPDH	GCACCGTCAAGGCTGAGAAC	TGGTGAAGACGCCAGTGGA
TGF beta 1 (TGFB)	TACCTGAACCCGTGTTGCTCTC	GTTGCTGAGGTATCGCCAGGAA
Arginase 1 (ARG1)	TCATCTGGGTGGATGCTCACAC	GAGAATCCTGGCACATCGGGAA
MCP1 (CCL2)	AGAATCACCAGCAGCAAGTGTCC	TCCTGAACCCACTTCTGCTTGG
IL10	TCTCCGAGATGCCTTCAGCAGA	TCAGACAAGGCTTGGCAACCCA

Intracellular calcium measurement

Intracellular Ca2+ was determined using the Fluo-4 Calcium Assay Kit (Beyotime) according to the manufacturer's instructions. Fluorescence was measured using a plate reader (Agilent BioTek Synergy Neo2 #N2MABT-SN).

References and Notes:

1. Békés, M., Langley, D.R., and Crews, C.M. (2022). PROTAC targeted protein degraders: the past is prologue. Nat. Rev. Drug Discov. *21*, 181–200. https://doi.org/10.1038/s41573-021-00371-6.

2. Ge, J., Li, S., Weng, G., Wang, H., Fang, M., Sun, H., Deng, Y., Hsieh, C.-Y., Li, D., and Hou, T. (2025). PROTAC-DB 3.0: an updated database of PROTACs with extended pharmacokinetic parameters. Nucleic Acids Res. *53*, D1510–D1515. https://doi.org/10.1093/nar/gkae768.

3. Hinterndorfer, M., Spiteri, V.A., Ciulli, A., and Winter, G.E. (2025). Targeted protein degradation for cancer therapy. Nat. Rev. Cancer *25*, 493–516. https://doi.org/10.1038/s41568-025-00817-8.

4. Dale, B., Cheng, M., Park, K.-S., Kaniskan, H.Ü., Xiong, Y., and Jin, J. (2021). Advancing targeted protein degradation for cancer therapy. Nat Rev Cancer *21*, 638–654. https://doi.org/10.1038/s41568-021-00365-x.

5. Chirnomas, D., Hornberger, K.R., and Crews, C.M. (2023). Protein degraders enter the clinic - a new approach to cancer therapy. Nat. Rev., Clin. Oncol. *20*, 265–278. https://doi.org/10.1038/s41571-023-00736-3.

6. Wang, L., Zhang, W., Shao, Y., Zhang, D., Guo, G., and Wang, X. (2022). Analytical methods for obtaining binding parameters of drug-protein interactions: A review. Anal Chim Acta *1219*, 340012. https://doi.org/10.1016/j.aca.2022.340012.

7. Blay, V., Tolani, B., Ho, S.P., and Arkin, M.R. (2020). High-Throughput Screening: today's biochemical and cell-based approaches. Drug Discov Today *25*, 1807–1821. https://doi.org/10.1016/j.drudis.2020.07.024.

8. Martinez Molina, D., Jafari, R., Ignatushchenko, M., Seki, T., Larsson, E.A., Dan, C., Sreekumar, L., Cao, Y., and Nordlund, P. (2013). Monitoring drug target engagement in cells and tissues using the cellular thermal shift assay. Science *341*, 84–87. https://doi.org/10.1126/science.1233606.

9. Almqvist, H., Axelsson, H., Jafari, R., Dan, C., Mateus, A., Haraldsson, M., Larsson, A., Martinez Molina, D., Artursson, P., Lundbäck, T., et al. (2016). CETSA screening identifies known and novel thymidylate synthase inhibitors and slow intracellular activation of 5-fluorouracil. Nat Commun *7*, 11040. https://doi.org/10.1038/ncomms11040.

10. Martinez, N.J., Asawa, R.R., Cyr, M.G., Zakharov, A., Urban, D.J., Roth, J.S., Wallgren, E., Klumpp-Thomas, C., Coussens, N.P., Rai, G., et al. (2018). A widely-applicable high-

throughput cellular thermal shift assay (CETSA) using split Nano Luciferase. Sci Rep *8*, 9472. https://doi.org/10.1038/s41598-018-27834-y.

11. Perrin, F. (1926). Polarisation de la lumière de fluorescence. Vie moyenne des molécules dans l'etat excité. J. Phys. Radium *7*, 390–401. https://doi.org/10.1051/jphysrad:01926007012039000.

12. Hall, M.D., Yasgar, A., Peryea, T., Braisted, J.C., Jadhav, A., Simeonov, A., and Coussens, N.P. (2016). Fluorescence polarization assays in high-throughput screening and drug discovery: a review. Methods Appl Fluoresc *4*, 022001. https://doi.org/10.1088/2050-6120/4/2/022001.

13. Tranter, G.E. (2017). Fluorescence Polarization and Anisotropy☆. In Encyclopedia of Spectroscopy and Spectrometry (Third Edition), J. C. Lindon, G. E. Tranter, and D. W. Koppenaal, eds. (Academic Press), pp. 632–634. https://doi.org/10.1016/B978-0-12-409547-2.12686-1.

14. Hendrickson, O.D., Taranova, N.A., Zherdev, A.V., Dzantiev, B.B., and Eremin, S.A. (2020). Fluorescence Polarization-Based Bioassays: New Horizons. Sensors (Basel, Switzerland) *20*, 7132. https://doi.org/10.3390/s20247132.

15. Bosson, J., Gouin, J., and Lacour, J. (2014). Cationic triangulenes and helicenes: synthesis, chemical stability, optical properties and extended applications of these unusual dyes. Chem Soc Rev *43*, 2824–2840. https://doi.org/10.1039/c3cs60461f.

16. Bora, I., Bogh, S.A., Santella, M., Rosenberg, M., Sørensen, T.J., and Laursen, B.W. (2015). Azadioxatriangulenium: Synthesis and Photophysical Properties of Reactive Dyes for Bioconjugation. European J Org Chem *2015*, 6351–6358. https://doi.org/10.1002/ejoc.201500888.

17. Ferguson, B.Q., and Yang, D.C. (1986). Methionyl-tRNA synthetase induced 3'-terminal and delocalized conformational transition in tRNAfMet: steady-state fluorescence of tRNA with a single fluorophore. Biochemistry *25*, 529–539. https://doi.org/10.1021/bi00351a002.

18. Li, H., Xiao, Y., Li, Q., Yao, J., Yuan, X., Zhang, Y., Yin, X., Saito, Y., Fan, H., Li, P., et al. (2022). The allergy mediator histamine confers resistance to immunotherapy in cancer patients via activation of the macrophage histamine receptor H1. Cancer Cell *40*, 36-52.e9. https://doi.org/10.1016/j.ccell.2021.11.002.

19. Coskun, E., Tuna, G., Jaruga, P., Tona, A., Erdem, O., and Dizdaroglu, M. (2019). Identification and quantification of DNA repair protein poly(ADP ribose) polymerase 1 (PARP1) in human tissues and cultured cells by liquid chromatography/isotope-dilution tandem mass spectrometry. DNA Repair (Amst) *75*, 48–59. https://doi.org/10.1016/j.dnarep.2019.01.008.

20. Stolzenburg, S., Rots, M.G., Beltran, A.S., Rivenbark, A.G., Yuan, X., Qian, H., Strahl, B.D., and Blancafort, P. (2012). Targeted silencing of the oncogenic transcription factor SOX2 in breast cancer. Nucleic Acids Res *40*, 6725–6740. https://doi.org/10.1093/nar/gks360.

21. The roles of the reprogramming factors Oct4, Sox2 and Klf4 in resetting the somatic cell epigenome during induced pluripotent stem cell generation | Genome Biology | Full Text https://genomebiology.biomedcentral.com/articles/10.1186/gb-2012-13-10-251.

22. Wuebben, E.L., and Rizzino, A. (2017). The dark side of SOX2: cancer - a comprehensive overview. Oncotarget *8*, 44917. https://doi.org/10.18632/oncotarget.16570.

23. Zhang, J., Zhang, M., Huo, X.-K., Ning, J., Yu, Z.-L., Morisseau, C., Sun, C.-P., Hammock, B.D., and Ma, X.-C. (2023). Macrophage Inactivation by Small Molecule Wedelolactone via Targeting sEH for the Treatment of LPS-Induced Acute Lung Injury. ACS Cent Sci *9*, 440–456. https://doi.org/10.1021/acscentsci.2c01424.

24. Napolitano, S., Martini, G., Ciardiello, D., Del Tufo, S., Martinelli, E., Troiani, T., and Ciardiello, F. (2024). Targeting the EGFR signalling pathway in metastatic colorectal cancer. Lancet, Gastroenterol. Hepatol. *9*, 664–676. https://doi.org/10.1016/S2468-1253(23)00479-X.

25. Zhou, F., Guo, H., Xia, Y., Le, X., Tan, D.S.W., Ramalingam, S.S., and Zhou, C. (2025). The changing treatment landscape of EGFR-mutant non-small-cell lung cancer. Nat. Rev., Clin. Oncol. *22*, 95–116. https://doi.org/10.1038/s41571-024-00971-2.

26. Khan, S., Zhang, X., Lv, D., Zhang, Q., He, Y., Zhang, P., Liu, X., Thummuri, D., Yuan, Y., Wiegand, J.S., et al. (2019). A selective BCL-XL PROTAC degrader achieves safe and potent antitumor activity. Nat. Med. *25*, 1938–1947. https://doi.org/10.1038/s41591-019-0668-z.

27. Baxter, E.W., Graham, A.E., Re, N.A., Carr, I.M., Robinson, J.I., Mackie, S.L., and Morgan, A.W. (2020). Standardized protocols for differentiation of THP-1 cells to macrophages with distinct M(IFNγ+LPS), M(IL-4) and M(IL-10) phenotypes. J. Immunol. Methods *478*, 112721. https://doi.org/10.1016/j.jim.2019.112721.

28. Thurmond, R.L., Gelfand, E.W., and Dunford, P.J. (2008). The role of histamine H1 and H4 receptors in allergic inflammation: the search for new antihistamines. Nat. Rev. Drug Discov. *7*, 41–53. https://doi.org/10.1038/nrd2465.

29. Micaroni, M. (2010). The role of calcium in intracellular trafficking. Curr Mol Med *10*, 763–773. https://doi.org/10.2174/156652410793384204.

30. Weber, G. (1952). Polarization of the fluorescence of macromolecules. I. Theory and experimental method. Biochem J *51*, 145–155. https://doi.org/10.1042/bj0510145.

31. Weber, G. (1952). Polarization of the fluorescence of macromolecules. II. Fluorescent conjugates of ovalbumin and bovine serum albumin. Biochem J *51*, 155–167. https://doi.org/10.1042/bj0510155.

32. Photoelectric Method for the Measurement of the Polarization of the Fluorescence of Solutions | CoLab https://colab.ws/articles/10.1364%2Fjosa.46.000962.

33. Patel, M.N., Halling-Brown, M.D., Tym, J.E., Workman, P., and Al-Lazikani, B. (2013). Objective assessment of cancer genes for drug discovery. Nat. Rev. Drug Discov. *12*, 35–50. https://doi.org/10.1038/nrd3913.

34. Henley, M.J., and Koehler, A.N. (2021). Advances in targeting "undruggable" transcription factors with small molecules. Nat. Rev. Drug Discov. *20*, 669–688. https://doi.org/10.1038/s41573-021-00199-0.

35. Yin, H., and Flynn, A.D. (2016). Drugging membrane protein interactions. Annu Rev Biomed Eng *18*, 51–76. https://doi.org/10.1146/annurev-bioeng-092115-025322.

Acknowledgments: We thank Xiaomi Lu, Siyuan Wang, and the Shenzhen Bay Laboratory Drug Discovery Core for experimental assistance. We also thank Dr. Yaoqi Zhou for his feedback on the manuscript.

Funding: This work was supported by the Shenzhen Bay Laboratory Open Fund, SZBL2021080601003; Shenzhen Bay Laboratory Proof of Concept Grant S231801006 (J.L.T.).

Author contributions: Conceptualization: J.L.T., Q.T.; Methodology: Q.T., Y.W.; Investigation: Q.T., Y.W., R.M., N.W., T.Z.Z., H.K.H., Z.I.B., I.I.; Supervision: X.L., J.W.P.Y., Y.H.W., Q.W., J.L.T.; Writing – original draft: Q.T., Y.W., R.M., J.L.T.; Writing – review & editing: Q.T., J.L.T.

Competing interests: J.L.T., Q.T., and Y.W. are co-inventors on a patent application filed by Shenzhen Bay Laboratory relating to work in this manuscript. The remaining authors disclose no conflicts.

Figures:

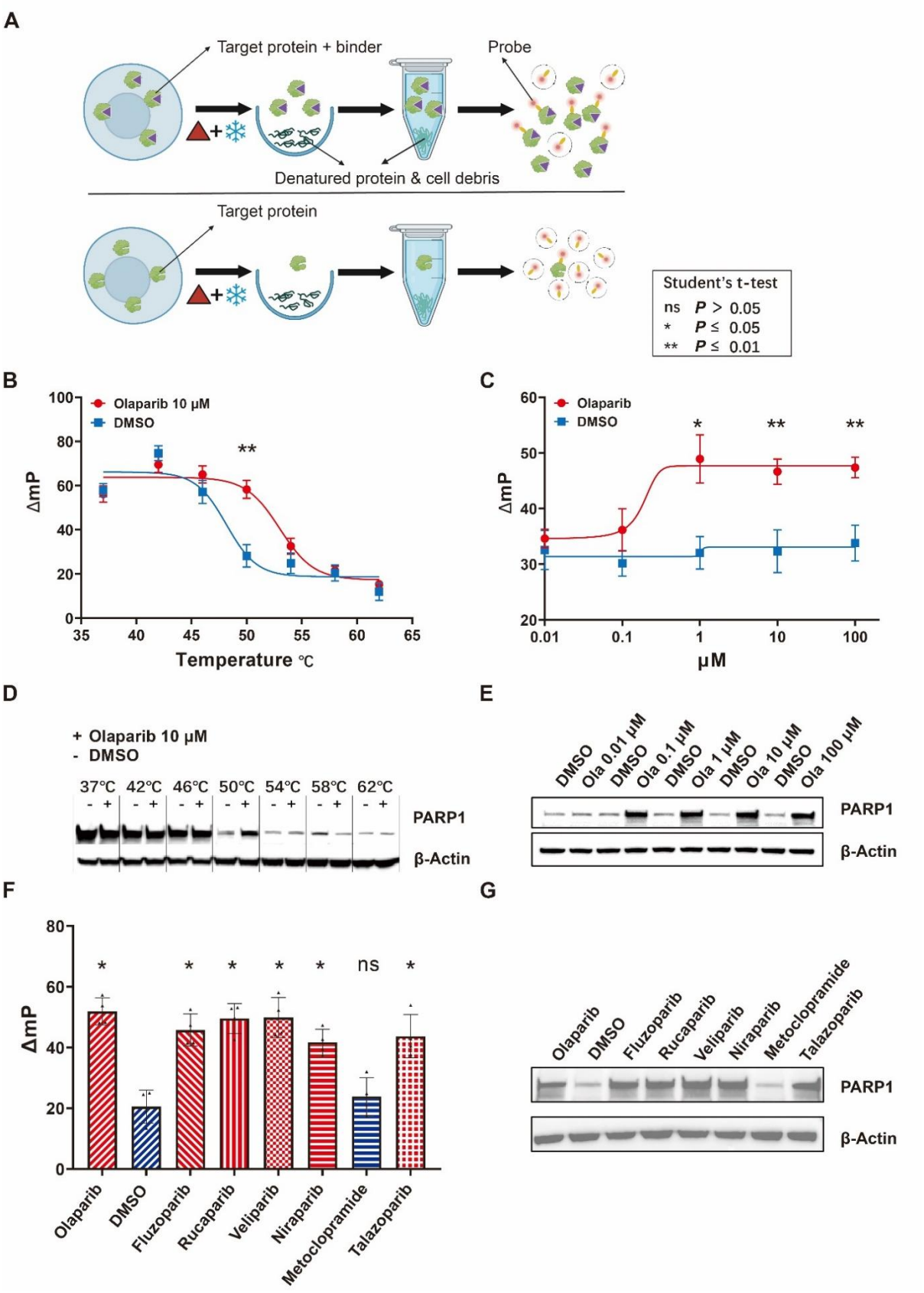

Fig. 1. CFAST detects binding of known PARP1 inhibitors to cellular PARP1. (A) Schematic diagram of CFAST. Created with BioRender.com/m62x513. **(B)** CFAST measurements of PARP1 probe in DMSO- and olaparib-treated HEK293T cell lysate, heated at various temperatures. **(C)** Dose-response CFAST measurements of PARP1 probe in DMSO- and olaparib-treated HEK293T cell lysate, heated at 50 ℃. **(D)** CETSA Western blot of PARP1 and ACTB in DMSO- and olaparib-treated HEK293T cells, heated at various temperatures. **(E)** Dose-response CETSA Western blot of PARP1 and ACTB in DMSO- and olaparib-treated HEK293T cells, heated at 50 ℃. **(F)** CFAST measurements of PARP1 in HEK293T cells incubated with DMSO and metoclopramide negative controls, and known PARP1 inhibitors, heated at 50 ℃. P-values are calculated relative to the DMSO group. **(G)** CETSA Western blot for PARP1 and ACTB in HEK293T cells treated with the same drugs in **F**, heated at 50 ℃. ΔmP values were obtained by normalizing to CFAST measurements of EGFP probe added to aliquots of experimental samples. Data are presented as mean ± SD, n = 5.

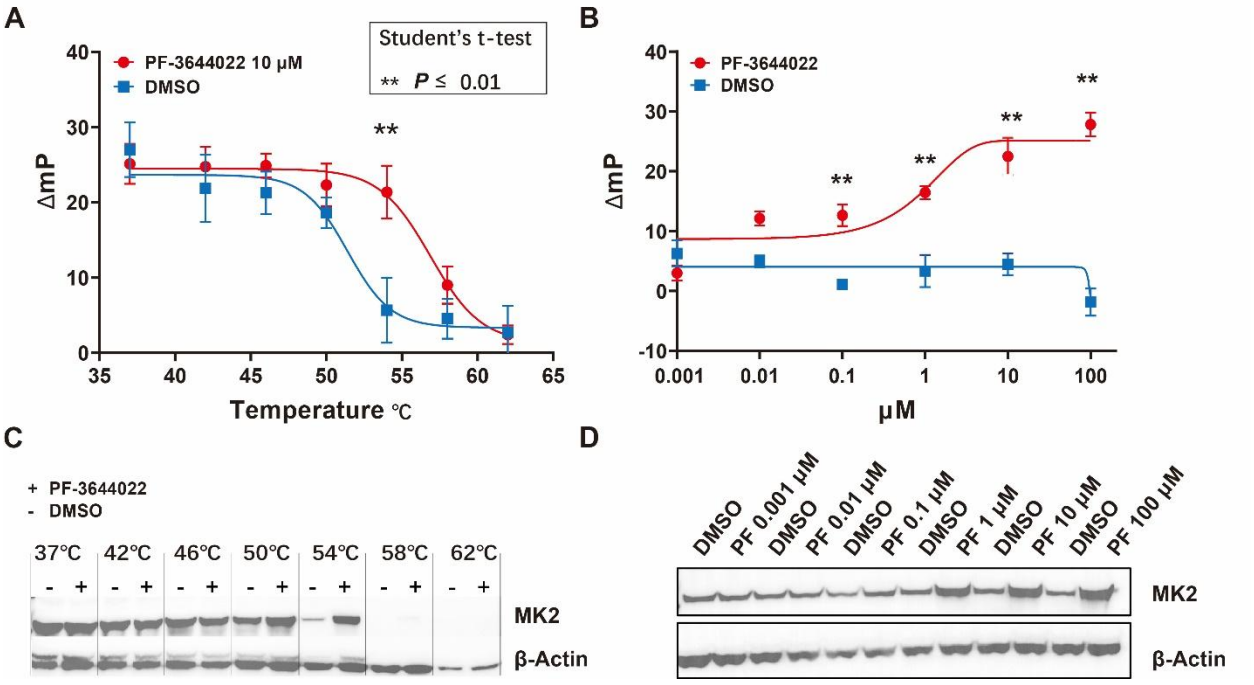

Fig. 2. CFAST detects binding of an MK2 inhibitor to cellular MK2. (A) CFAST measurements of MK2 probe in DMSO- and PF-3644022-treated HEK293T expressing MK2 cell lysate, heated at various temperatures. **(B)** Dose-response CFAST measurements of MK2 probe in DMSO- and PF-3644022-treated HEK293T expressing MK2 cell lysate, heated at 54 ℃. **(C)** CETSA Western blot of MK2 and ACTB in DMSO- and PF-3644022-treated HEK293T expressing MK2 cells, heated at various temperatures. **(D)** Dose-response CETSA Western blot of MK2 and ACTB in DMSO- and PF-3644022-treated HEK293T expressing MK2 cells, heated at 54 ℃. ΔmP values were obtained by normalizing to CFAST measurements of EGFP probe added to aliquots of experimental samples. Data are presented as mean ± SD, n = 5.

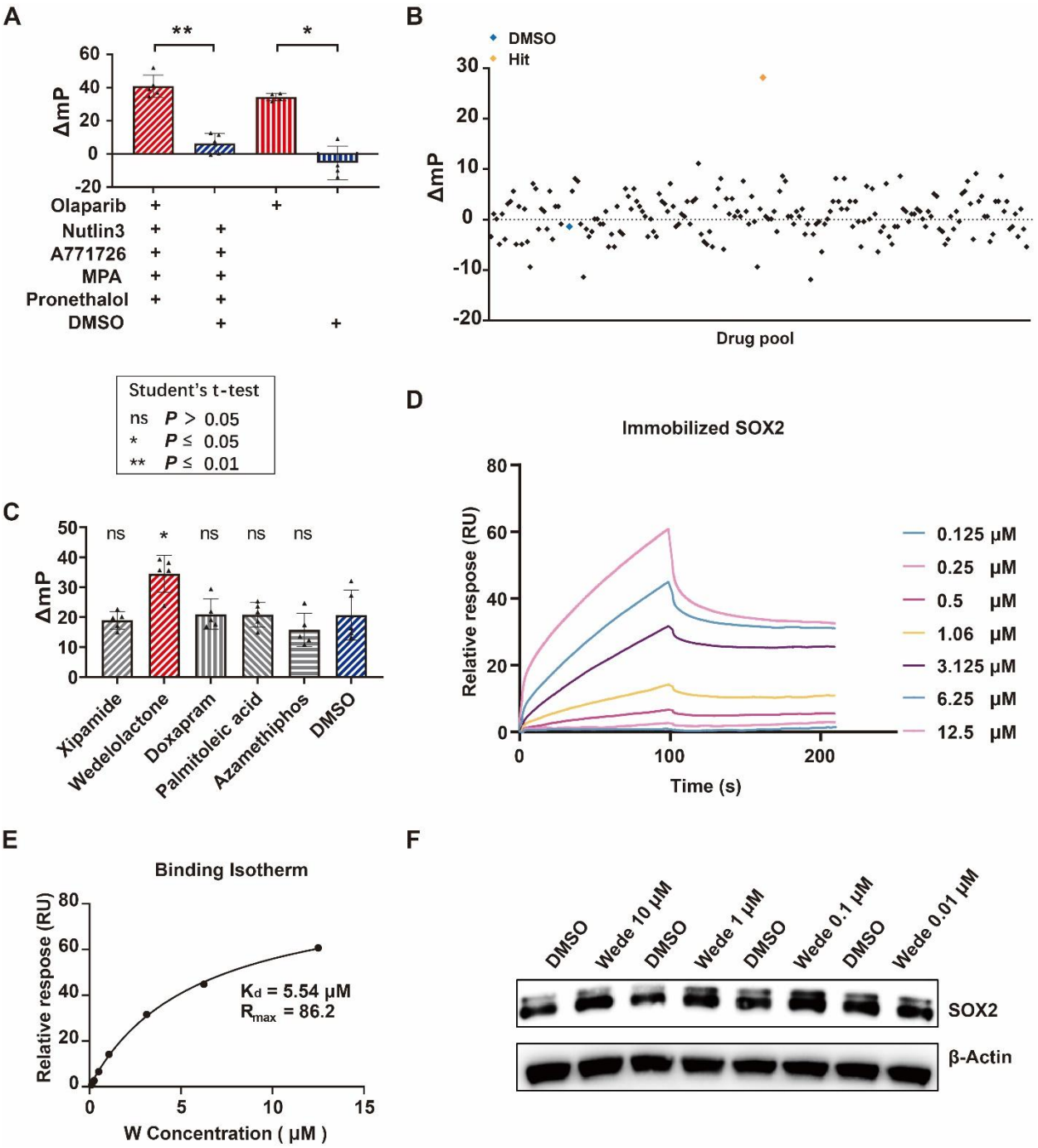

Fig. 3. CFAST screening identifies a novel small molecule binder of SOX2. (A) CFAST measurements of PARP1 probe in HEK293T cells incubated with 10 μM of various small molecule combinations, heated at 58 °C. Data are presented as mean ± SD, n = 5 **(B)** High throughput CFAST measurements of MYC-tag probe in HEK293T cells expressing MYC-tag SOX2 incubated with 900 small molecules in pools of 5, heated at 58 °C. Values are the average of 2 replicates, n = 2. **(C)** CFAST for SOX2 in HEK293T *Tg:SOX2* cells treated with drugs from the pooled hit at 10 μM, heated at 58 °C. P-values are calculated relative to the DMSO group. Data are presented as mean ± SD, n = 5. **(D, E)** Dose-response surface plasmon resonance measurements of wedelolactone and recombinant SOX2 protein interaction. ΔmP values were obtained by

normalizing to CFAST mP measurements of EGFP probe added to an aliquot of experimental samples. **(F)** Dose-response CETSA Western blot of SOX2 and ACTB in DMSO- and wedelolactone-treated H69 cells, heated at 58 °C.

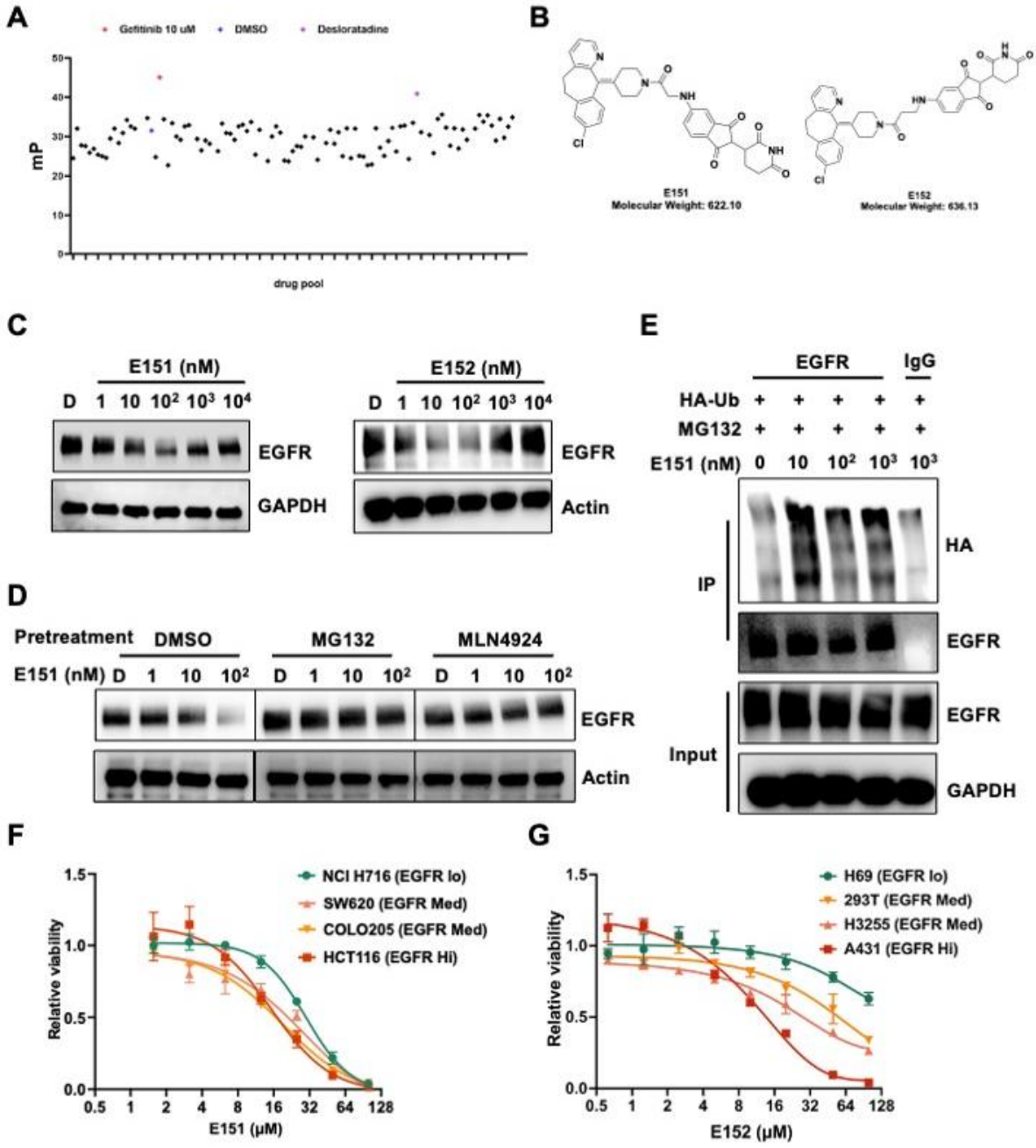

Fig. 4. Desloratadine warhead PROTACs target EGFR. (A) High throughput CFAST measurements of MYC-tag probe in HEK293T cells expressing MYC-tag EGFR incubated with 900 small molecules in pools of 5, heated at 50 °C. **(B)** Chemical structures of PROTACs E151 and E152 with desloratadine warheads. **(C)** Dose-response western blot of EGFR, GAPDH, and Actin in DMSO-, E151- and E152-treated A431 cells. **(D)** Dose-response western blot of EGFR and Actin of DMSO- and E151-treated A431 cells pretreated with DMSO, proteasome inhibitor MG132, or neddylation inhibitor MLN4924. **(E)** Immunoprecipitation of EGFR and HA-tagged ubiquitin in A431 cells treated with MG132 and E151. GAPDH serves as loading control. **(F)** Cell viability of E151-treated colorectal cancer cell lines with variable EGFR expression. Data are presented as mean ± SD, n = 3. **(G)** Cell viability of E152 treatment in various cancer cell lines with variable EGFR expression. Data are presented as mean ± SD, n = 3.

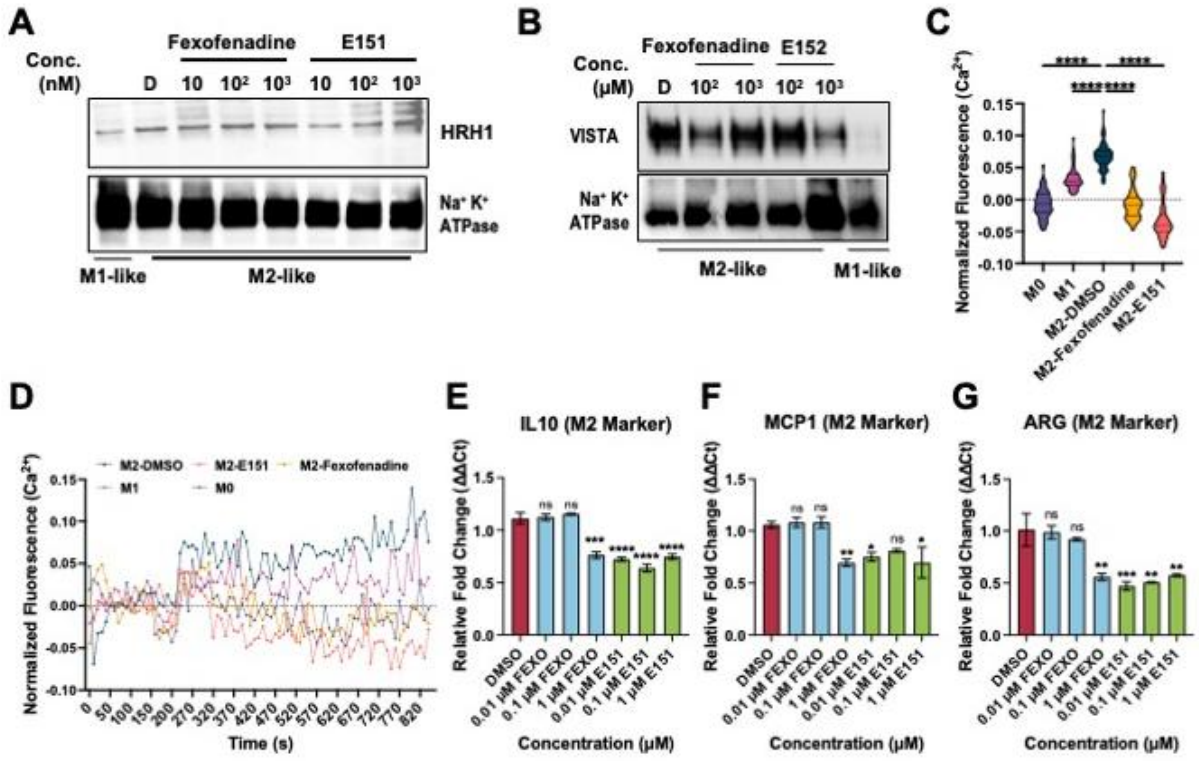

Fig. 5. Desloratadine warhead PROTACs inhibit HRH1 to reprogram immune cells. (A,B) Western blot of membrane fraction HRH1, VISTA, and Na^+/K^+ ATPase from M1-like or M2-like THP-1 induced macrophages treated with fexofenadine, E151, or E152. **(C,D)** Mobilization of intracellular calcium (Fluo-4 assay) of THP-1 induced M0, M1-like, and drug treated M2-like macrophages stimulated with 10 μM histamine stimulation from 180 s, n = 3. The violin plot summarizes the distribution of fluorescence proportional to intracellular calcium intensity. Significance was computed by one-way ANOVA. **(E-G)** qRT-PCR determined relative mRNA level of M2 macrophage markers (IL-10, MCP1, ARG) in DMSO-, fexofenadine-, or E151-treated M2-like macrophages. Significance was computed by one-way ANOVA.